Microstructural records of multiple retrograde local H_2O supplement in the pelitic gneiss, Lützow-Holm Complex at Akarui Point, East Antarctica

AYA NAKAMURA[1], MASAO KITAMURA[1] AND TETSUO KAWAKAMI[1, *]

[1] Department of Geology and Mineralogy, Graduate School of Science, Kyoto University, Kitashirakawa Oiwake-cho, Sakyo-ku, Kyoto 606-8502, Japan

* Corresponding author,
E-mail; t-kawakami@kueps.kyoto-u.ac.jp

Published as

Nakamura, A., Kitamura, M. & Kawakami, T. 2014, Microstructural records of multiple retrograde local H_2O supplement in the pelitic gneiss, Lützow-Holm Complex at Akarui Point, East Antarctica. *Mineralogy and Petrology*, **108**, *177-186*.

ABSTRACT

The alkali-feldspar and biotite in the sillimanite-biotite-garnet gneiss from East Antarctica preserves characteristic microstructural evidence of multi-stage H_2O supplement during the retrograde metamorphism. The first microstructural evidence is the 'zoned feldspar', in which the mesoperthitic zone, the anti-perthitic zone and lamella-free plagioclase zone coexist within a single crystal. They are occasionally found next to biotite, and are always depleted in orthoclase (Or) component toward the biotite. The formation process of this microstructure could be explained by the diffusion that oversteps the solvus. The second microstructural evidence is the serrate boundary between alkali-feldspar and biotite. The projections of biotite are selectively developed next to Or lamellae of alkali-feldspar every 3-5 μm. These two microstructures would have formed as the biotite grew by consuming potash in alkali-feldspar when H_2O-bearing fluid locally passed through the grain boundaries. The former microstructure was formed at 825-900 ^{o}C before lamella formation, and the latter microstructure was formed after the lamella formation. These microstructures are the indicators of fluid pathways formed under two different temperature conditions. The common coexistence of these microstructures implies that the fluid used similar pathways during the retrograde metamorphism.

Keywords: diffusion, ternary feldspar, fluid, solvus, serrate grain boundary

INTRODUCTION

Fluid plays an important role in geologic processes through mass and heat transfer. It also defines mechanical strength of rocks, density, and volatile content, thus elastic properties of rocks (Jamtveit and Austrheim, 2010). Fluid infiltration can trigger the metamorphic reactions (Austrheim, 1987) or partially affect the isotopic composition of geochronologically important minerals such as zircon and monazite (Geisler et al., 2007; Kawakami and Suzuki, 2011; Williams et al., 2011) or assist new growth of such minerals (Kirkland et al., 2009). Therefore, recognition of the fluid activity and determination of its timing during metamorphism is crucial for the correct interpretation of the results from dating as well as the pressure-temperature-time (*P-T-t*) path.

Fluid activity in metamorphic rocks is commonly preserved as microstructures involving hydrous minerals, such as garnet partly replaced by the biotite due to retrograde hydration reactions. This kind of retrograde hydration is a common phenomenon in most metamorphic rocks. Although multiple fluid activity with different fluid compositions is likely (e.g., Higashino et al., 2013), determination of the timing at which fluid infiltration took place has been difficult to constrain especially for high-temperature (upper-amphibolite to granulite facies conditions, including ultrahigh-temperature condition) where most of the mineral compositions are commonly altered by the later diffusion processes.

Ternary feldspars, however, can preserve chemical evidence of high-temperature conditions if the original single-phase composition can be calculated from the lamella microstructure, even for ultrahigh-temperature metamorphic rocks (e.g., Hokada, 2001). Utilizing this method for ternary feldspars with zonal, lamellar microstructures potentially serve as a record of chemical zoning formed at high temperatures. In this study, we utilize unique microstructures of ternary feldspars and biotite as a recorder of fluid activity in the high-temperature metamorphic rocks and show how these can be interpreted.

ANALYTICAL METHOD

Chemical analysis of constituent minerals and the X-ray elemental mapping were performed with the JEOL JXA8105 at Kyoto University. The analytical conditions for the quantitative analyses were 15 kV accelerating voltage, 10 nA probe current, 3 μm beam diameter and counting time of 10 and 5 seconds for peaks and backgrounds

respectively for most elements, and 30 and 15 seconds, respectively, for F and Cl. Natural and synthesized oxides were used as standards, and the ZAF correction was employed for processing the X-ray intensity data. Aluminosilicates were identified by Raman spectroscopy (JASCO NRS 3100) at Kyoto University. Several back scattered electron images were obtained using the field emission-scanning electron microscope (JEOL JMS-7001) at Osaka University.

In order to calculate the pre-exsolution composition of feldspars, chemical analyses of the host feldspar and lamella, coupled with their relative proportions, were utilized based on the methodology described in Kroll et al. (1993) and Hokada (2001). The areal proportions of host feldspar and lamella were estimated utilizing back scattered electron (BSE) images and an image processing software 'Image J' (Rasband, 2007). Areal proportion was assumed to be identical to the volume proportion, and the weight proportion was calculated utilizing densities of 2.67 g/cm^3 for albite (Ab) and 2.57 g/cm^3 for orthoclase (Or). The celcian component (< 0.6 mol%) and ferric iron (< 0.1 mol%) was neglected because of low concentrations.

SAMPLE DESCRIPTION

The sample utilized in this study is a sillimanite-biotite-garnet gneiss (sample TK2002122304) collected from the Lützow-Holm Complex at Akarui Point during the 44th Japan Antarctic Research Expedition (JARE). It occurs intercalated with the biotite-hornblende gneiss. The peak metamorphic condition of 7.7-9.8 kbar and 770-790 ^oC was previously estimated from the same sample (Kawakami et al., 2008). For further details of the geological setting and sample locality, see Kawakami et al. (2008).

The studied sample mainly consists of garnet porphyroblasts, alkali-feldspar, plagioclase, quartz, biotite and sillimanite (Fig. 1a-c), with minor amounts of ilmenite, spinel, rutile, apatite, monazite and zircon. The sample can be divided into two parts. In the pinkish 'leucosome' lenses and layers, alkali-feldspar, quartz and garnet are dominant. In the residuum white-colored part with melanocratic patches, garnet, biotite and alkali-feldspar are dominant (Fig. 1a). The leucosome is concordant with the gneissosity, which is mainly defined by biotite ± sillimanite (Fig. 1a, c).

Garnet ($Alm_{62-75}Prp_{19-26}Grs_{1-16}Sps_{1-2}$, X_{Mg} [= $Mg/(Mg + Fe_{total})$] = 0.20-0.28) occurs as porphyroblast of up to ca. 10 mm in diameter (Fig. 1a-b). It commonly accompanies pressure shadows of the leucosome (Fig. 1a), suggesting that at least part

of the garnet rim is a peritectic product of partial melting and the leucosome originally represents the melt (Vernon and Clarke, 2008). The garnet is chemically zoned, and the X_{Mg} value increases from the core to the rim, suggesting its prograde origin. The garnet core includes some rare inclusions of anorthite(An)-rich plagioclase (An_{30-50}) compared to that in the matrix. The rim includes biotite, quartz, plagioclase (An_{12-16}), and kyanite. A kyanite inclusion in the rim supports a prograde origin of garnet because the kyanite is considered to be the prograde relic (e.g., Hiroi et al., 1983).

Feldspars in the matrix can be divided into three types; ternary feldspar with Or-rich alkali-feldspar rim (Figs. 2a-c, 3); plagioclase (An_{2-15}; Fig. 2a); and 'zoned feldspar' (Fig. 2d). The distribution of these three types of feldspars can best be recognized by X-ray element maps (Fig. 3). Although Fig. 3 mainly covers the residuum part, thin-section-scale element mapping showed that three types of feldspars are present in both the leucosome and the residuum.

Alkali-feldspar is coarse-grained (up to ~3 mm) and characterized by the strong development of exsolution lamellae (Fig. 2a-c). In general, each grain consists of an inner region with a mesoperthitic microstructure and an outer region with a perthitic microstructure (Fig. 3). Some grains of alkali-feldspar consist of a region with only perthitic microstructure (Figs. 2a-b, 3). Since they are smaller than those with mesoperthitic and perthitic regions, their appearance can be explained by preferential cutting during the fabrication of the thin section. They also could be small grains of mesoperthite re-equilibrated to form perthite and matrix plagioclase during retrograde metamorphism (see below). The change from mesoperthitic domain to perthitic domain is microstructurally gradual (Fig. 2b), and thus the integrated feldspar composition varies gradually as well. Reintegration of the exsolution microstructures shows that the inner region of the alkali-feldspar has the intermediate composition of Ab and Or with 1-2 wt% CaO, and that the outer regions has an Or-richer and An-poorer composition compared to the inner region (Table 1). The former is termed 'ternary feldspar' and the latter 'Or-rich alkali-feldspar' hereafter for simplicity. The width of the lamellae in the ternary feldspar (mesoperthitic regions) varies from 3 to 10 μm. Commonly, both fine (~3 μm) and coarse (~10 μm) lamellae coexist in a single alkali-feldspar core (Fig. 2b), although domains with only fine lamellae or coarse lamellae are also present. The proportion of Ab lamellae between these two domains is very similar, suggesting that pre-exsolution single-phase composition of these domains were almost the same. Fine

lamellae, especially, are not perfectly straight although they are almost uniform in width (Fig. 2b), and they occasionally bifurcate. Therefore, this mesoperthitic microstructure is considered to have formed through spinodal decomposition.

Plagioclase (An_{2-15}) is commonly present in the matrix along the grain boundaries between the alkali-feldspar (Figs. 2a, 3), or surrounding biotite aggregate (Fig. 3c). Plagioclase contains more An content (~An_{15}) when surrounding a biotite aggregate, whereas those present between alkali-feldspar grains as films are more albitic and vary in composition (An_{2-10}) (Fig. 3c). Very albitic plagioclase (An_{2-3}) tends to be concentrated at the rim of the plagioclase films developed between alkali-feldspar grains (Fig. 3c). Where Or-rich alkali feldspar is finer grained and abundant, the plagioclase is abundant along the grain boundaries, suggesting a genetic relationship (Fig. 3).

Zoned feldspar is commonly observed next to biotite at the biotite-rich portion of the matrix. The occurrence of this type of feldspar is rare, and shows a localized distribution on the thin section scale. The following three zones coexist in each zoned feldspar grain: (i) zone 1 with mesoperthitic microstructure, (ii) zone 2 with anti-perthitic microstructure, and (iii) zone 3 consisting of albitic plagioclase without lamellae (Fig. 2d). Zoned feldspar lacking zone 3 is rarely present. The microstructure and pre-exsolution composition of zone 1 are, in most cases, quite similar to that of the ternary feldspar. Therefore, this zone remained almost unaffected by the formation of the zonal structure, retaining the original, high-temperature composition. The lamellae in the zone 1 are considered to have formed as a result of spinodal decomposition. Zone 2 has microstructural features interpreted to have formed as a result of spinodal decomposition, such as lamellae uniform in width but incompletely straight (Figs. 2d, 4a).

Textural correlation between zoned feldspar and biotite

Zoned feldspar is commonly developed next to matrix biotite. Towards the biotite, the feldspar changes from zone 1 through zone 2 to zone 3. In order to detect the original chemical zoning that was formed before the lamellar microstructures, an integrated composition for the long rectangular areas in Fig. 4a were estimated (termed ‘line traverse analysis’ hereafter) and the result is plotted in Fig. 4b. The overall trend in the recalculated single-phase feldspar composition is to become depleted in the Or

component as biotite is approached. The change in composition from zone 1 to zone 2 is discontinuous, while in many cases, the lamellae are continuous at the boundary between zones 1 and 2 (Fig. 4a). Within each zone, the recalculated pre-exsolution composition varies as a function of distance from the adjacent biotite (Fig. 4b). The pre-exsolution composition of the reintegrated areas in the zone 1 is occasionally enriched in the Or component near the boundary between zones 1 and 2. In zone 2, the Or component decreases near the boundary between zones 1 and 2 (Fig. 4b).

When the adjoining biotite is at a high angle with respect to the Or lamella in alkali-feldspar, the boundary between the alkali-feldspar and the biotite is often serrated. Each of the biotite projections are selectively developed next to the Or lamella every 3-5 μm. In addition the thickness of the Or lamellae often gradually decreases towards the biotite (Fig. 5). These biotite projections are not developed next to the Ab lamella. When the lamellae in alkali-feldspar are at a low angle with the adjoining biotite, this kind of projection also does not occur. It should be noted that the development of this serrate boundary is a phenomenon which requires a smaller scale of mass transfer than the zoned feldspar formation as discussed below.

DISCUSSION

Prograde to peak metamorphism

Since the garnet in this study was formed during the prograde metamorphism, the minerals found as inclusions in the garnet rim, biotite, kyanite, garnet, quartz, alkali-feldspar and plagioclase (An_{12-16}), represent the mineral assemblage of the prograde stage. The peak *P-T* conditions estimated using the same sample as this study (7.7-9.8 kbar and 770-790 ^{o}C; Kawakami et al., 2008) uses the garnet grains that include sillimanite in the rim. Therefore, garnet porphyroblast growth continued from the kyanite stability field into the sillimanite stability field in the sample used in this study.

Mesoscopic microstructure, such as the development of leucosome (Fig. 1a), both as lenses and pressure shadows of garnet, indicates that the sample experienced partial melting, and that the garnet is the peritectic product of the partial melting reaction. Replacement of the garnet rim by the intergrowth of biotite and plagioclase (Fig. 1b) is a characteristic of a microstructure representing the back reaction between garnet and melt during cooling (Holness et al., 2011a). Therefore, it is highly likely that melt was

present at the peak of metamorphism, and the melt forming reaction is likely to be

Bt + Als (Ky/Sil) + Qtz → Grt + Akfs + melt.

Since the studied sample is very rich in the Or component, the Akfs component was not only incorporated into the melt but also existed as a solid phase during the peak metamorphism.

Formation of ternary feldspar and Or-rich alkali-feldspar rim

The pre-exsolution compositions of the alkali-feldspars are plotted on the An-Ab-Or ternary diagram of Fuhrman and Lindsley (1988) (Figs. 4 and 6). The ternary feldspar (Fig. 6) and zone 1 of the zoned feldspar (Fig. 4) preserves the highest temperature among the feldspars of the sample at the isotherm for 750-900 ^{o}C, with the majority around 825 ^{o}C, suggesting that the ternary feldspar was formed at 825-900 ^{o}C (Figs. 4 and 6). This temperature range is slightly higher than the peak metamorphic temperature of Akarui Point previously estimated as 770-790 ^{o}C (Kawakami et al. 2008). This suggests that the ternary feldspar was stable at the peak of metamorphism.

Orthoclase-rich alkali-feldspar developed at the rim of the ternary feldspar can be interpreted to have coexisted with plagioclase (~An_{10}) present at the grain boundaries. This mineral assemblage is the same as that consisting of the host and exsolution lamella in the ternary feldspar. The An content of the matrix plagioclase is almost the same as that of the plagioclase lamella (Fig. 6; Table 1), except for the case of extremely albitic plagioclase in the matrix (An_{2-3}). In addition, the composition of the Or-rich alkali-feldspar mostly plots on the 750 ^{o}C isotherm near the Ab-Or join (Fig. 6). These observations indicate that the Or-rich alkali-feldspar was formed at lower temperature than the ternary feldspar.

As described above, the development of the Or-rich alkali-feldspar rim on the ternary feldspar is not concentric, indicating a formation mechanism other than the overgrowth. Furthermore, the ternary feldspar compositions are on the tie line between the Or-rich alkali-feldspar composition and most of the grain boundary film plagioclase (Fig. 6). These observations suggest that the Or-rich alkali-feldspar and the matrix plagioclase (except for extremely albitic ones) formed as a result of ternary feldspar decomposition during cooling. That is, the core/rim relationship between the ternary and Or-rich alkali-feldspars in a single grain can be explained by the diffusion of the Ab and An components toward matrix plagioclase nucleated at the grain boundaries.

Another possible mechanism to account for the formation of the Or-rich alkali-feldspars may be an interface-coupled dissolution-precipitation mechanism (e.g., Lobotka et al., 2004; Putnis and Putnis, 2007, Niedermeier et al., 2009), because we assume the presence of low H_2O activity [$a(H_2O)$] fluid around the Or-rich alkali-feldspars as discussed in the next section. Lobotka et al. (2004) shows an example of Ab replaced by Or as a result of this mechanism. In the present case, the change from mesoperthitic domain to perthitic domain is microstructurally gradual (Fig. 2b), which is inconsistent with the sharp boundary expected to form by the interface-coupled dissolution-precipitation mechanism. Extremely albitic plagioclase in the matrix could be the product of the final stage fluid infiltration.

After formation of the Or-rich alkali-feldspar during cooling, the ternary feldspar that survived from the depletion of the An and Or components must have experienced spinodal decomposition to form the current lamellar microstructure. After further cooling, Or-rich alkali-feldspar areas must have exsolved. Differences in the thickness and periodicity of these lamellar microstructures support this order.

Formation of the zoned feldspar

Zoned feldspar (Fig. 2d) shows two features different from the other alkali-feldspar grains; (i) It is found only in grains adjacent to biotite, and (ii) the Or component of the re-integrated grain composition decreases at those feldspar rims in contact with biotite, from zone 1 to zone 3 (Fig. 4). The re-integrated compositions from each zone of the feldspar (Table 2) plot approximately on a straight line corresponding to X-$Or_{75}Ab_{25}$ in the An-Ab-Or ternary diagram (Fig. 4c), where X is a composition at which a gray broken line crosses the Ab-An apex..

Ternary feldspar could have formed originally at a temperature of 825-900 ^oC as discussed above. At 825-900 ^oC, an H_2O-bearing fluid infiltrated along the grain boundaries between ternary feldspar and biotite that was already present in the matrix (Fig. 4a). New biotite was then formed by consuming H_2O component in the fluid and Or component from the ternary feldspar. This reaction was the driving force responsible for the diffusion profile shown in Fig. 4b (roughly from point 20 to point 5, except for the points 15-10 formed after the formation of zones 1 and 2). The diffusion profile only slightly oversteps the solvus at 825 ^oC, such the diffusion profile is smooth (a thick gray line of Fig. 4b). As shown by the similar mean diffusion distance during the zoned

299 feldspar formation, reaction (1) took place at the right-hand side of Fig. 4a (corresponds
300 to point 4 to point 1 of Fig. 4b) under similar temperature conditions, and produced
301 another diffusion profile.
302 If the infiltrating H_2O-bearing fluid was near pure H_2O, it will trigger partial
303 melting. This is because the temperature estimated is higher than 825 ^oC, well above the
304 water-saturated solidus for the pelitic rocks (e.g. Spear et al., 1999). However, the
305 preservation of such a high-temperature microstructure is consistent with the infiltration
306 of a low a(H_2O) fluid such as CO_2-rich fluid or the F- and/or Cl-bearing fluid (e.g.,
307 Higashino et al., 2013) that prevented partial melting, but acted as a source of H_2O. It is
308 likely that biotite formed where the a(H_2O) in the fluid was relatively high. The fluid
309 only promoted the material transport at the grain boundaries to form the plagioclase film
310 along the grain boundaries where a(H_2O) in the fluid was low.
311 The observation that compositional variation in the zoned feldspar is not aligned
312 on the X-Or(Bt) tie line but shifted to the more albitic side (X-$Or_{75}Ab_{25}$) implies that the
313 Ab component was lost from the ternary feldspar into the fluid phase at the same time
314 the Or component went to form biotite (Fig. 4c). This release of the Ab component
315 might have been driven by a reaction between An-rich plagioclase that was present in
316 the matrix during near-peak metamorphic conditions as indicated by the plagioclase
317 inclusions in the garnet rim (An_{12-16}). Another possible source for an Ab component in
318 the fluid is the plagioclase included in the prograde garnet core (An_{30-50}; Fig. 6) that was
319 released to the matrix via partial breakdown of the garnet (Fig. 1b).
320 With further temperature decrease, the compositional trend formed by the diffusion
321 processes oversteps the solvus; for example, the trend X-$Or_{75}Ab_{25}$ in Fig. 4c crosses the
322 solvus at 825 ^oC. It is at this stage that the large compositional gap between zones 1 and
323 2, as shown by the broken lines in Fig. 4b, was created.
324 The fact that compositions of the zoned feldspar (zones 1, 2 and 3), matrix
325 plagioclase (~An_{10}), and Or-rich alkali-feldspar are aligned on a single trend, and the
326 fact that the composition of the Or-rich alkali-feldspar preserves the composition
327 characteristic of the 750 ^oC isotherm (Figs. 4 and 6) suggest that formation of these
328 major microstructures was complete by 750 ^oC. The composition near the solvus for the
329 Ab-Or join at ~700 ^oC ($Ab_{27.5}Or_{71.8}An_{0.8}$; Table 1) is preserved as the Or phase of the
330 Or-rich alkali-feldspar. Preservation of such a composition, without changing to more
331 Or-rich composition is rare (cf. Hokada, 2001), and requires a rapid cooling process

after their formation.

Further decrease in temperature diminished the mean diffusion distance for the biotite-forming reaction at the boundary between biotite and the zone 3. This resulted in the elimination of zone 1 such that zone 1 no longer consumed Or component. However, consumption of the Or component by zone 2 continued. Finally at relatively lower temperatures, the local equilibrium at the zone 1/ zone 2 boundary caused the zone 1 side to become Or-richer and the zone 2 side to become Ab-richer. Further consumption of the Or component probably resulted in zone 3.

Lamella formation in zones 1 and 2 by spinodal decomposition probably started to take place at the minimal and maximal of the Or component in zones 1 and 2, respectively (point 9 of zone 1 and point 16 of zone 2), because the fast cooling forces these compositions to hit the spinodal curve first. The lamella formation probably propagated to the surrounding compositions as a temperature decrease.

The interface-coupled dissolution-precipitation mechanism may potentially be applicable to the formation of the zoned feldspar. The important microstructural constraint in applying this mechanism is that the zoned feldspar is only found adjacent to biotite. Therefore, biotite and zoned feldspar should have a genetic link, and probably formed simultaneously when a fluid infiltrated between them. However, since biotite is not included in the zoned feldspar, and the zoned feldspar is not porous, we consider that microstructural observation does not necessarily support that the interface-coupled dissolution-precipitation occurred in the present case.

As a conclusion, the zoned feldspar described in this study is a rare case where the formation process could be explained by the diffusion that oversteps the solvus (e.g., Sekerka and Wang, 1999).

Formation of serrate boundary between biotite and feldspar

The boundary between biotite and feldspar is rarely serrated. Where it occurs the projections of biotite are selectively developed next to the Or phase (Fig. 5). This microstructural feature implies that serrated boundary formation postdated the lamella formation, and that Or lamella and the projections of biotite have some genetic relationship. Because the Or lamellae in contact with the biotite projections are thinner near the contact with biotite (Fig. 5), this boundary likely formed by the consumption of Or to form biotite (Fig. 4), or in other words, dissolution of Or to recrystallize biotite

through the reaction

Or + (H_2O in $fluid_1$) + (Fe, Mg from garnet or $fluid_1$)

= Bt + Ab + ($fluid_2$). ……(2)

Although biotite projections at the serrate boundary are too small to perform quantitative analyses, their textural features indicate a very short diffusion distance and suggest that they developed during the final stage of biotite formation during retrograde metamorphism.

Abart et al. (2009) reports similar microstructure as above, which is the Ab/Or interface within the mesoperthite in an anatexite from Tanzania, corrugated on the sub-micron scale; lobes of Or extend into more An-rich lamellae within the Ab host. This is interpreted as growth phenomenon associated with coarsening of the Or lamellae, that took place after Ab lamella exsolved about the peristerite gap (Abart et al., 2009). Different from the serrate boundary between biotite and feldspar, this microstructure lacks apparent evidence for the presence of fluid during its formation, such as the presence of hydrous mineral.

Holness et al. (2007; 2011b) also reports similar microstructure (‘stepped grain boundary’) from the Skaergaard Intrusion, East Greenland, where clinopyroxene/plagioclase grain boundaries have serrations associated with the dissolution of exsolution lamellae from Ca-poor pyroxene, and the corresponding growth of Ca-rich plagioclase is observed. Non-ubiquity of the serrated boundaries on the thin-section scale, and their association with larger, non-isochemical, symplectic structures, suggests that they formed by the dissolution of metastable Ca-poor pyroxene and recrystallization of adjacent plagioclase and augite consequent to the introduction of a metasomatizing fluid along grain boundaries (Holness et al., 2007). Therefore, similar fluid-related process observed in the solidified layered intrusion is likely to have taken place in the course of solidification of partially molten high-temperature metamorphic rocks as well. By understanding the mechanism of these microstructure formation discussed above, these microstructures will serve as a tool to detect the fluid related processes in high-temperature rocks.

ACKNOWLEDGEMENTS

We would like to thank R. Abart and anonymous reviewer for constructive reviews. Previous version of this manuscript was improved by the comments by D. Harlov. We

would also like to thank the JARE members for the supports during the field work and discussion, A. Tsuchiyama for permitting the usage of FE-SEM, and S. Ohi for assistance. A.N. thanks T. Hoshide for discussion. This research was supported by the Grant-in-Aid for Young Scientists (B) (19740326, 23740391) from JSPS to T.K.

REFERENCES CITED

Abart, R., Petrishcheva, E., Rhede, D., and Wirth, R. (2009) Exsolution by spinodal decomposition: II: perthite formation during slow cooling of anatexites from Ngornghoro, Tanzania. American Journal of Science, 309, 450-475.

Austrheim, H. (1987) Eclogitization of lower crustal granulites by fluid migration through shear zones. Earth and Planetary Science Letters, 81, 221-232.

Elkins, L.T. and Grove, T.L. (1990) Ternary feldspar experiments and thermodynamic models. American Mineralogist, 75, 544-559.

Fuhrman, M.L. and Lindsley, D.H. (1988) Ternary feldspar Modeling and thermometry. American Mineralogist, 73, 201-215.

Geisler, T., Pidgeon, R.T., Kurtz, R., Van Brownswijk, W. and Schleicher, H. (2003) Experimental hydrothermal alteration of partially metamict zircon. American Mineralogist, 88, 1496-1513.

Higashino, F., Kawakami, T., Satish-Kumar, M., Ishikawa, M., Maki, K., Tsuchiya, N., Grantham, G. and Hirata, T. (2013) Chlorine-rich fluid activity during granulite facies metamorphism in the Late Proterozoic to Cambrian continental collision zone – an example from the Sør Rondane Mountains, East Antarctica. Precambrian Research, *in press*.

Hiroi, Y., Shiraishi, K., Nakai, Y., Kano, T. and Yoshimura, S. (1983) Geology and petrology of Prince Olav Coast, East Antarctica. Antarctic Earth Science, 32-35.

Hokada, T. (2001) Feldspar thermometry in ultrahigh-temperature metamorphic rocks: Evidence of crustal metamorphism attaining ~1100 ^{o}C in the Archean Napier Complex, East Antarctica. American Mineralogist, 86, 932-938.

Hokada, T. and Suzuki, S. (2006) Feldspar in felsic orthogneiss as indicator for UHT crustal processes. Journal of Mineralogical and Petrological Sciences, 101, 260-264.

Holness, M.B., Cesare, B. and Sawyer, E.W. (2011a) Melted rocks under the microscope: Microstructures and their interpretation. Elements, 7, 247-252.

Holness, M.B., Stripp, G., Humphereys, M.C.S., Veksler, I.V., Nielsen, T.F.D. and Tenger, C. (2011b) Silicate liquid immiscibility within the crystal mush: Late-stage magmatic microstructures in the Skaergaard Intrusion, East Greenland. Journal of Petrology, 52, 175-222.

Holness, M.B., Tenger, C., Nielsen, T.F.D., Stripp, G. and Morse, S.A. (2007) A textural record of solidification and cooling in the Skaergaard Intrusion, East Greenland. Journal of Petrology, 48, 2359-2377.

Kawakami, T., Grew, E.S., Motoyoshi, Y., Shearer, C.K., Ikeda, T., Burger, P.V. and Kusachi, I. (2008) Kornerupine sensu stricto associated with mafic and ultramafic rocks in the Lützow-Holm Complex at Akarui Point, East Antarctica: what is the source of boron? Geological Society, London, Special Publications, 308, 351-375.

Kawakami, T. and Hokada, T. (2010) Linking P-T path with development of discontinuous phosphorus zoning in garnet during high-temperature metamorphism — an example from Lützow-Holm Complex, East Antarctica. Journal of Mineralogical and Petrological Sciences, 105, 175-186.

Kawakami, T. and Suzuki, K. (2011) CHIME monazite dating as a tool to detect polymetamorphism in high-temperature metamorphic terrane – an example from the Aoyama area, Ryoke metamorphic belt, SW Japan. Island Arc, 20, 439-453.

Kirkland, C.L., Whitehouse, M.J. and Slagstad, T. (2009) Fluid-assisted zircon and monazite growth within shear zone: a case study from Finnmark, Arctic Norway. Contributions to Mineralogy and Petrology, 158, 637-657.

Kretz R (1983) Symbols for rock-forming minerals. American Mineralogist, 68, 277-279.

Kroll, H., Evangelakakis, C. and Voll, G. (1993) Two-feldspar geothermometry: a review and revision for slowly cooled rocks. Contributions to Mineralogy and Petrology, 114, 510-518.

Labotka, T.C., Cole, D.R., Fayek, M., Ricipti, L.R., Stadermann, F.J. (2004) Coupled cation and oxygen-isotope exchange between alkali feldspar and aqueous chloride solution. American Mineralogist, 89,1822-1825.

Luth, W.C. (1974) Analysis of experimental data on alkali feldspars;unit cell parameters and solvi. In: MacKenizie W.S. and Zussman J. (Eds.), The Feldspars. Manchester University Press, Manchester, 249-296.

Niedermeier D.R. D., Putnis A, Geisler T, Golla-Schindler U and Putnis C.V. (2009)

The mechanism of cation and oxygen isotope exchange in alkali feldspars under hydrothermal conditions. Contributions to Mineralogy and Petrology, 157, 65-76.

Putnis A and C. V. Putnis (2007) The mechanism of reequilibration of solids in the presence of a fluid phase. Journal of Solid State Chemistry, 180, 1783-1786.

Raase, P. (1998) Feldspar thermometry: a valuable tool for deciphering the thermal history of granulite-facies rocks, as illustrated with metapelites from Sri Lanka. The Canadian Mineralogist, 36, 67-86.

Sawyer, E.W. (2008) Atlas of Migmatites. The Canadian Mineralogist, Special Publication 9. NRC Research Press, Ottawa, Ontario, Canada. 371p.

Sekerka, R. F., and Wang, S.L. (1999) The moving phase boundary problems. In: Aaronson, H. I. ed., Lectures on the theory of phase transformations, 2nd edition. TMS, Warrendale, Pennsylvania, 231-284.

Spear, F.S., Kohn, M.J. and Cheney, J.T. (1999) P-T paths from anatectic pelites. Contributions to Mineralogy and Petrology, 134, 17-32.

Vernon, R.H. and Clarke, G.L. (2008) Principles of Metamorphic Petrology, Cambridge University Press, New York, 446p.

FIGURE CAPTIONS

FIGURE 1. (a) A slab photo of the sample TK2002122304. Dark gray spots are the garnet porphyroblasts and melanocratic patches are mainly biotite and sillimanite. Leucosome is developed as layer-parallel lenses or as the pressure shadows of garnet. **(b)** A back scattered electron (BSE) image showing the biotite replacing garnet with plagioclase, and biotite included in the garnet rim. **(c)** A BSE image showing the mode of occurrence of coarse-grained, biotite and prismatic sillimanite enclosed in a plagioclase moat. Finer grained biotite occurs as a matrix mineral in the alkali-feldspar- and quartz-dominant portion. **(d)** Photomicrograph (crossed polarized light) of the biotite and zoned feldspars surrounding it. **(e)** Enlargement of the boxed area in **(d)**. Cross polarized light. Note that the zoned feldspar (contoured with a solid line) shows the same grey retardation except for white lamellae, suggesting that the zoned feldspar, as a whole, is a single crystal. The gray and white parts in the zoned feldspar correspond to the Ab phase and Or phase, respectively. The zoned feldspar crystal changes its composition from an Or-rich one to almost pure albitic plagioclase at the contact with

biotite. Mineral abbreviations are after Kretz (1983) except for the followings: Ilm = ilmenite, Afs = alkali-feldspar, Pl = plagioclase and Z.F. = zoned feldspar.

FIGURE 2. (a)-(d) Feldspar BSE images. **(a)** Ternary feldspar and Or-rich alkali-feldspar in the matrix. Dark films at the grain boundaries between alkali-feldspar grains are albitic plagioclase. Note that Or-rich alkali-feldspar is finer grained than the ternary feldspars, and is locally developed at the rim of the ternary feldspar as well. They are both accompanied by the development of a plagioclase film at the grain boundaries. **(b)** Ternary feldspar has domains with fine-grained lamellae (indicated by 'fine') and coarse-grained lamellae (indicated by 'coarse') in a single grain. **(c)** Or-rich alkali-feldspar coexisting with biotite in the matrix. Its lamellae vary in width, but exceedingly fine-grained lamellae are uniformly distributed at the core of the grain. At the rim, the lamellae are partly absent under BSE image. Note the finer-grain size of the Or-rich alkali-feldspar compared to the ternary feldspar. **(d)** Mode of occurrence of the zoned feldspar. The zones 1, 2, and 3 are labeled as 1, 2, and 3, respectively. Zones with mesoperthitic microstructure (zone 1), anti-perthitic microstructure (zone 2) and lamella-free albitic plagioclase (zone 3) can be recognized. Toward the grains of biotite, each alkali-feldspar grain becomes depleted in the Or component.

FIGURE 3. Elemental mapping of the matrix (principally residuum). Warm colors represent high concentrations of each element. Note the mode of occurrence of ternary feldspar and the Or-rich alkali-feldspar rim. A plagioclase film is developed at the grain boundaries of the alkali-feldspars. (a) Elemental map of Na. (b) Elemental map of K. (c) Elemental map of Ca. (d) Back scattered electron image.

FIGURE 4. (a) A BSE image of the zoned feldspar showing the rectangular areas used to calculate the change in the modal proportion of Or phase (light gray) as a function of distance from the adjacent biotite. The modal proportion of the Or phase is determined in each rectangular area and the result is plotted in (b). The white broken line is a baseline for the measurement of distance from the biotite. Note that the thickness of the Or phase increases at the boundary between zones 2 and 1. Quartz at the bottom right is the matrix phase. **(b)** Change of the modal proportion of the Or component as a function of distance from biotite to zone 3. Gray thick line represents the diffusion profile

originally present in the pre-exsolution ternary feldspar. Note the sharp increase in the Or at the zone 1 /zone 2 boundary, which is interpreted to postdate zones 1 and 2 formation. **(c)** The An-Ab-Or ternary diagram for the pre-exsolution, re-integrated compositions for each of the three zones of the zoned feldspar, with isotherms at 750 ^{o}C, 825 ^{o}C, and 900 ^{o}C as shown by solid lines after Fuhrman and Lindsley (1988). Gray, broken line represents the tie line between the compositions of zone 3 and the Or-rich part of the zone 1.

FIGURE 5. (a) The BSE image of the serrated boundary between biotite and alkali-feldspar. The projections of biotite are selectively developed next to the Or lamellae (light gray) and not developed next to the Ab lamellae (dark gray). **(b)** Enlargement of the boxed area in (a). **(c)** An illustration showing the formation mechanism of serrated boundary between biotite and feldspar. See text for detailed explanation.

FIGURE 6. An-Ab-Or ternary diagram for recalculated pre-exsolution alkali-feldspar compositions, with the isotherms at 750 ^{o}C, 825 ^{o}C, and 900 ^{o}C are shown by the solid lines (after Fuhrman and Lindsley, 1988). Compositions of prograde plagioclase included in garnet and retrograde plagioclase in the matrix are also shown.

TABLE 1. Representative compositions of Or phase and Ab phase of ternary feldspar, Or-rich alkali feldspar and the zoned feldspar (zone 1, zone 2 and zone 3). Or; Or phase, Ab; Ab phase, S.D.; standard deviation.

TABLE 2. Summary of the reintegrated composition of zones 1 and 2 of the zoned feldspar and the result of temperature estimate utilizing the ternary feldspar thermometry by Fuhrman and Lindsley (1988) (FL) and Elkins and Grove (1990) (EG). The different characters in the ‘grain’ line represent the grain names of feldspar analyzed. The ‘Zone’ column shows the zone number of the zoned feldspar.

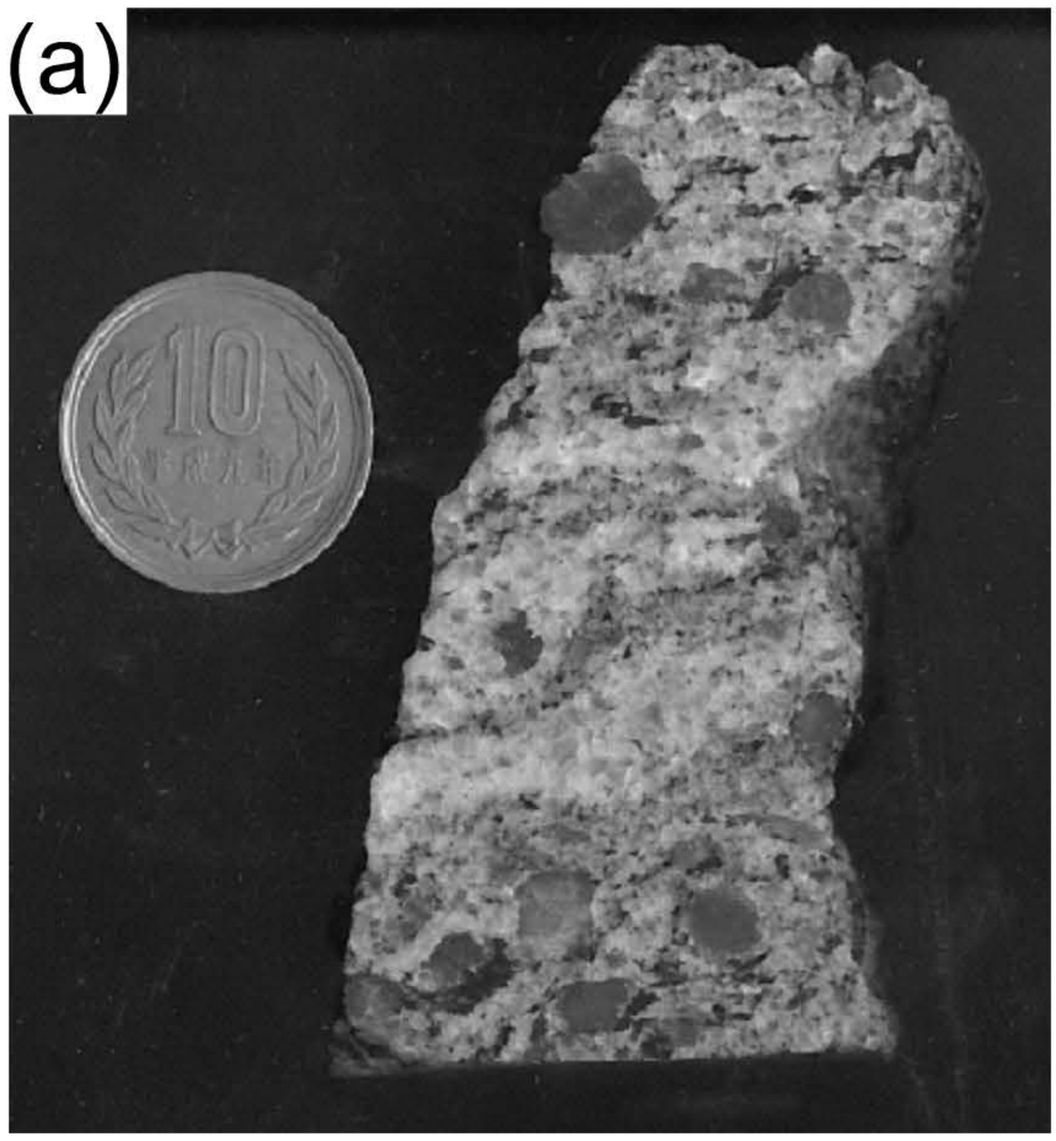

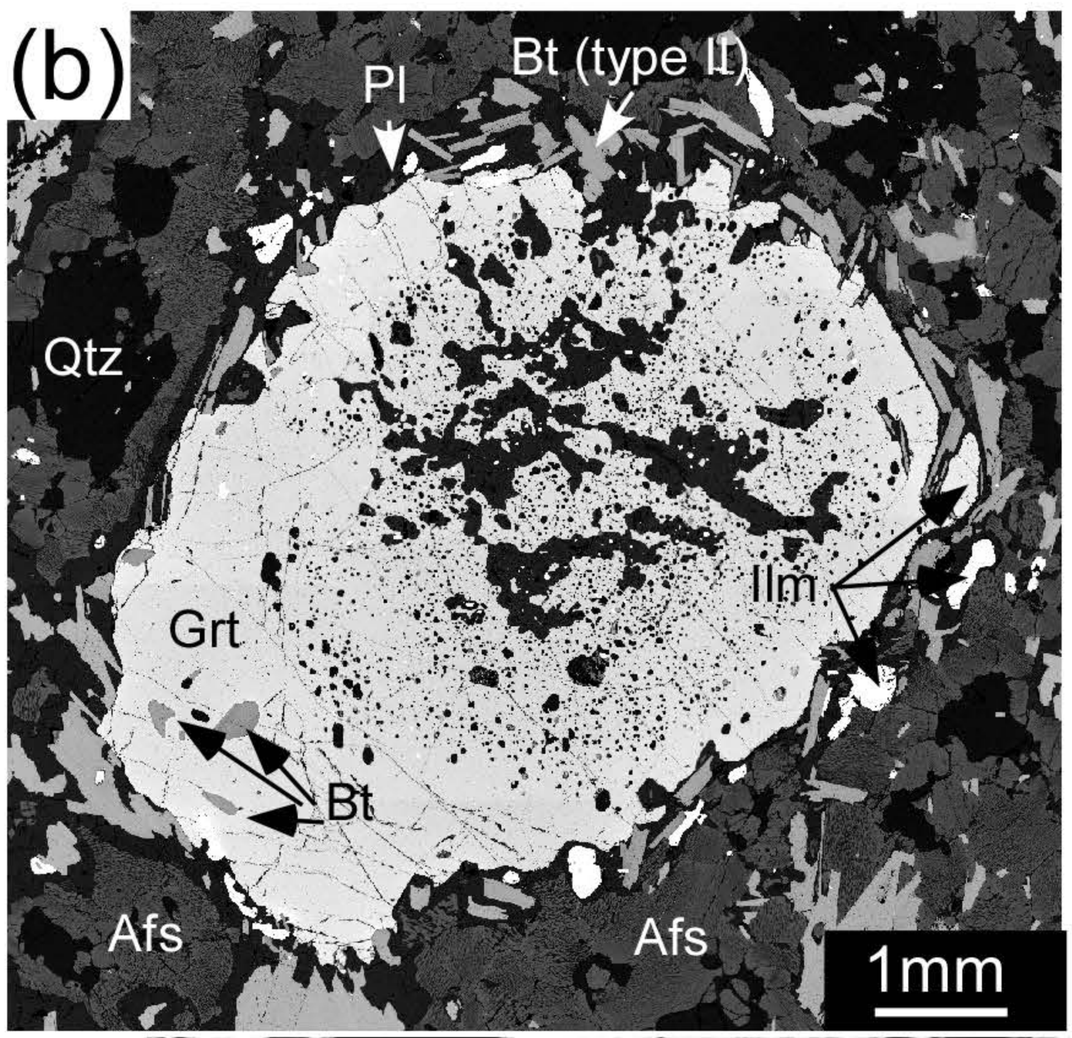

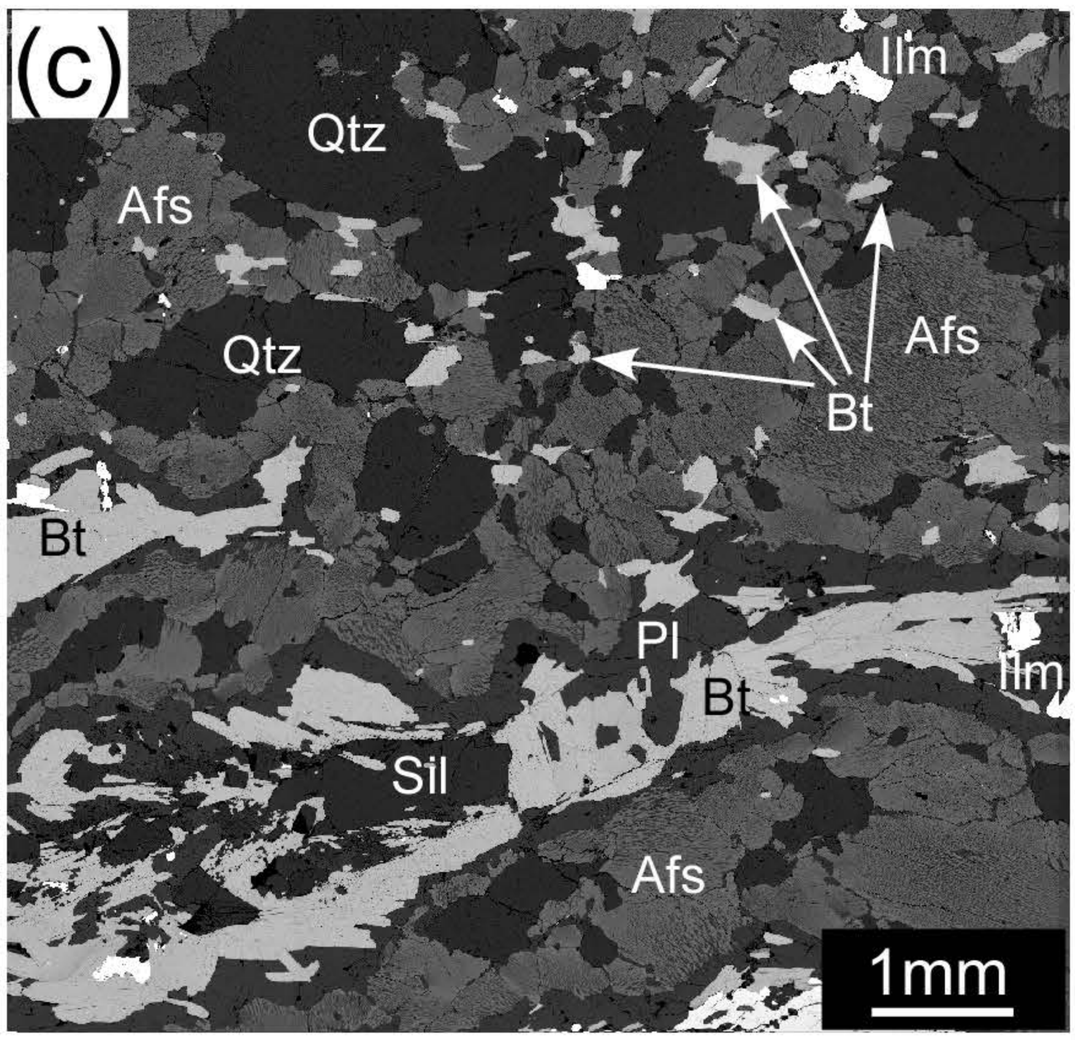

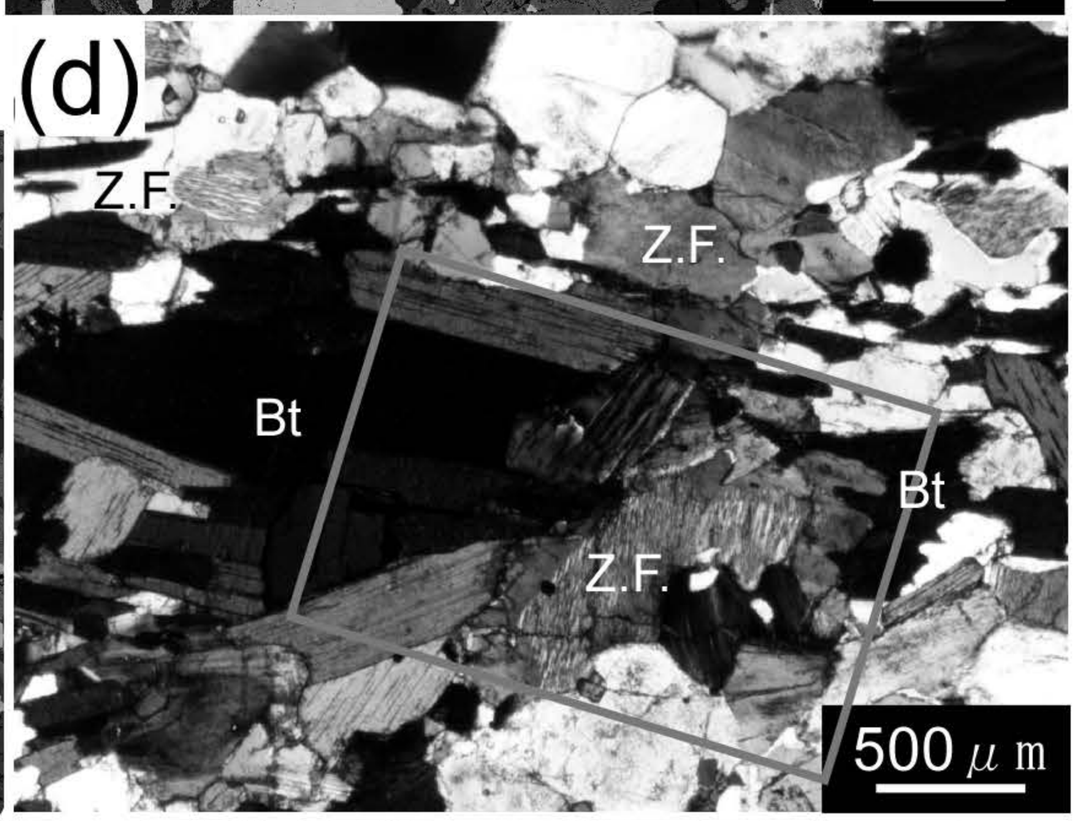

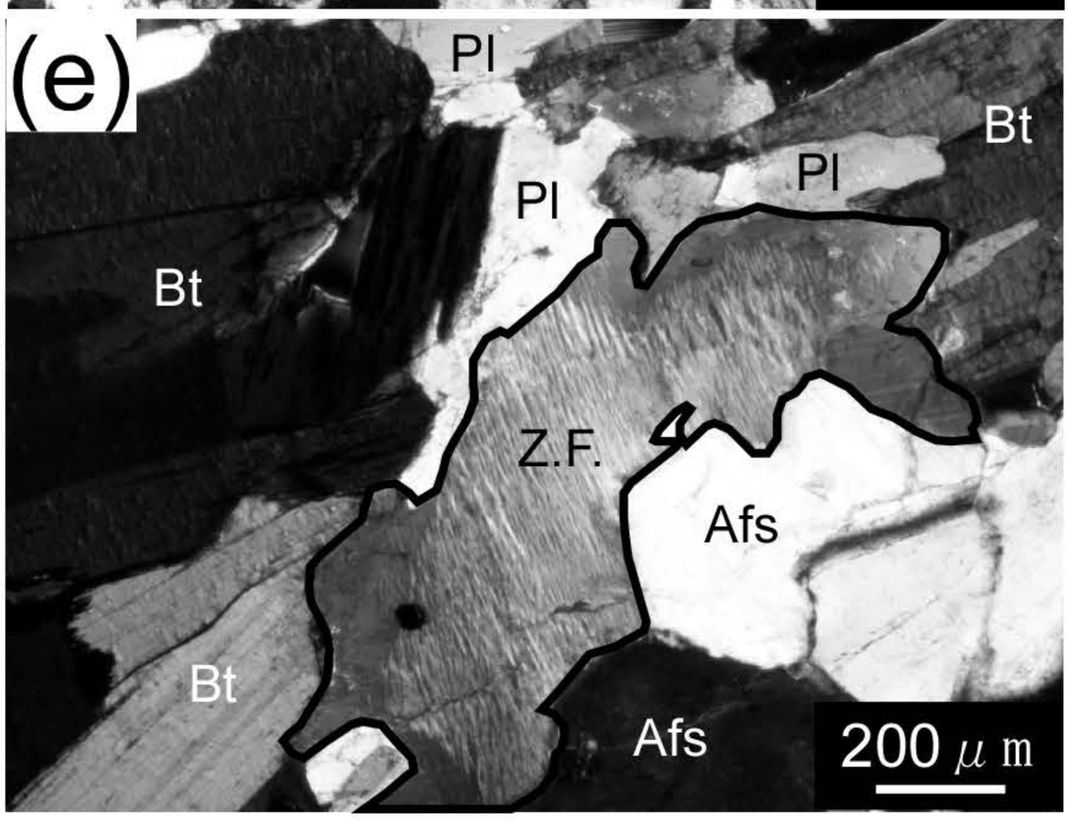

Nakamura et al. FIGURE 1

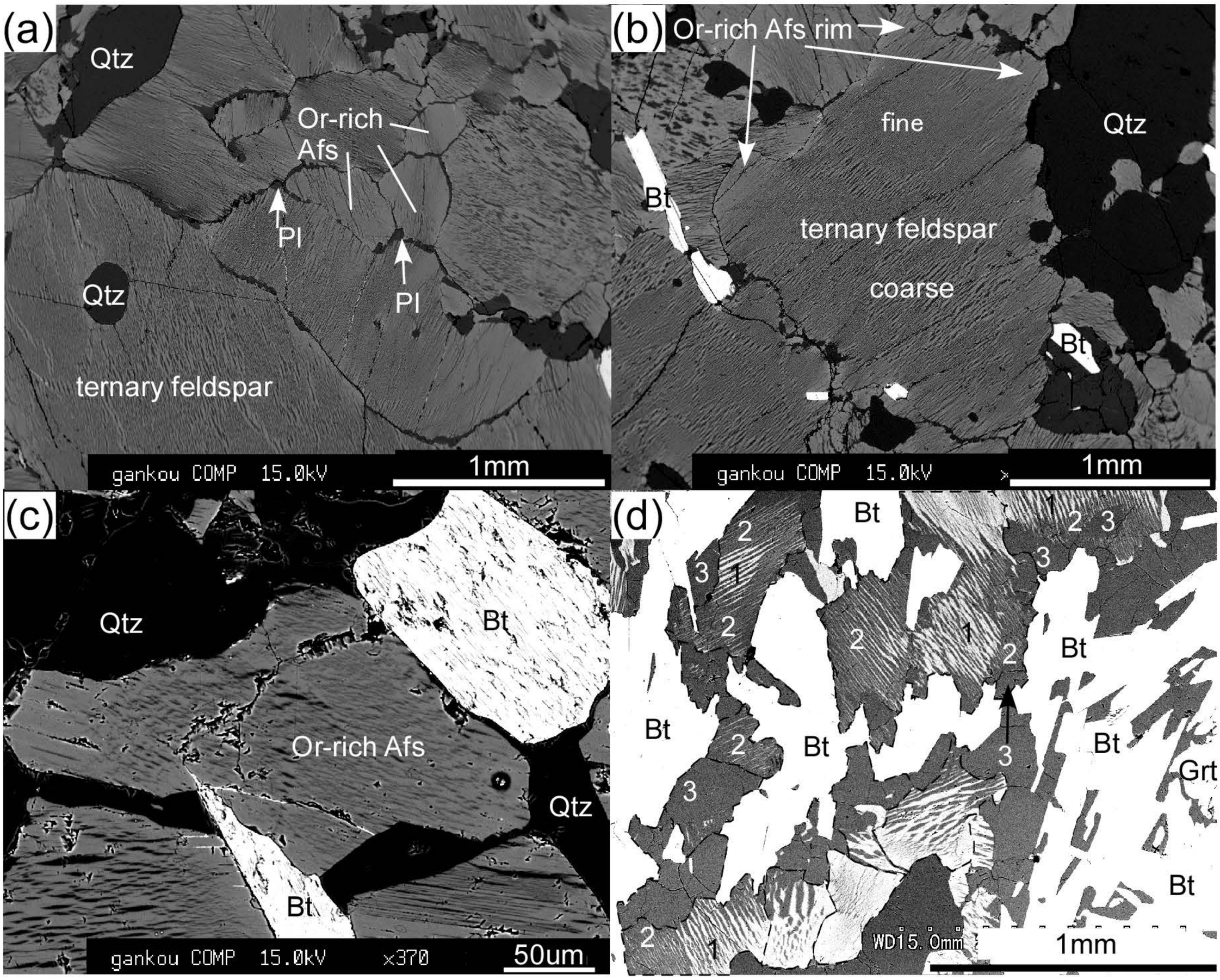

Nakamura et al FIGURE 2

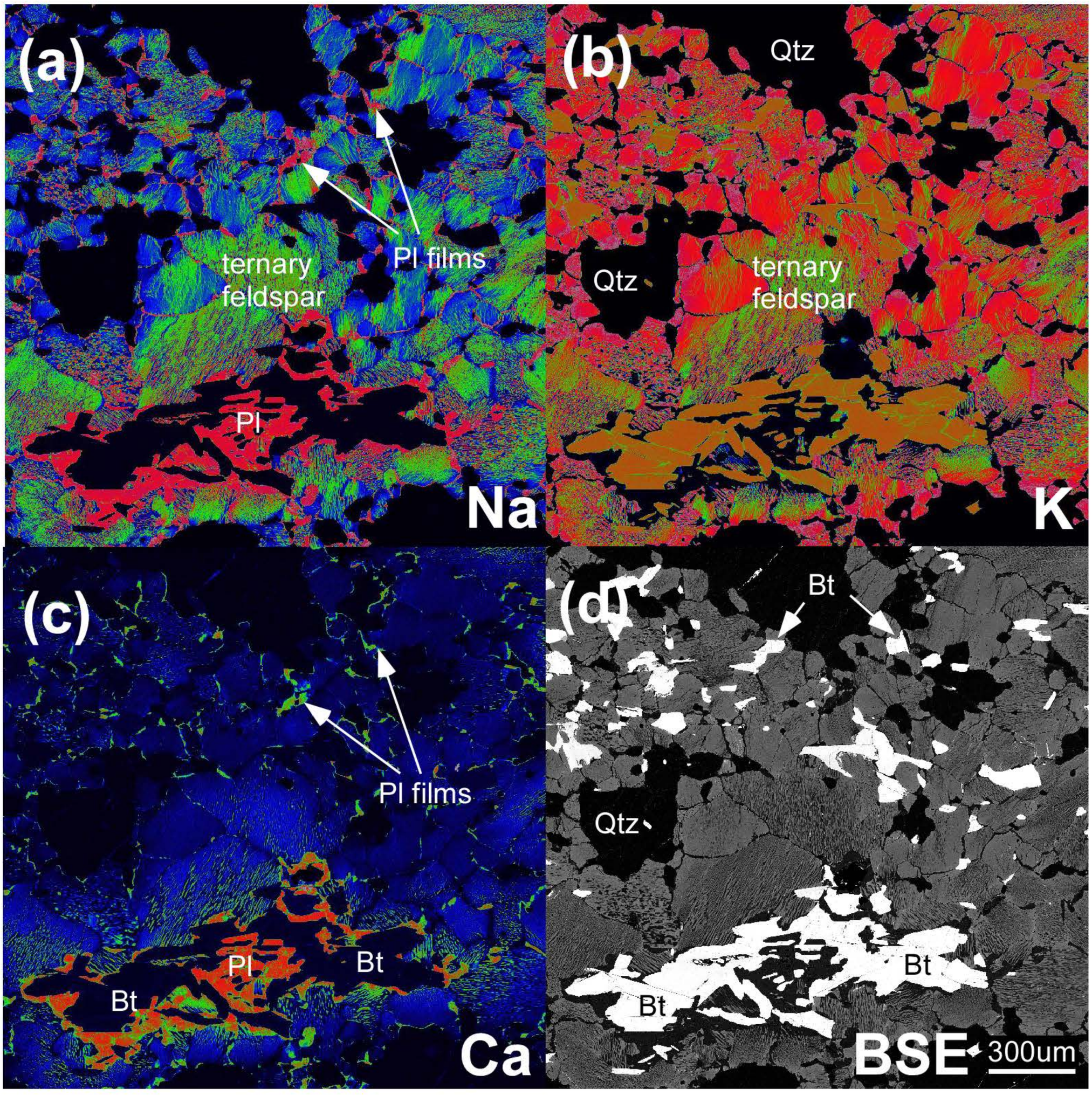

Nakamura et al Fig. 3

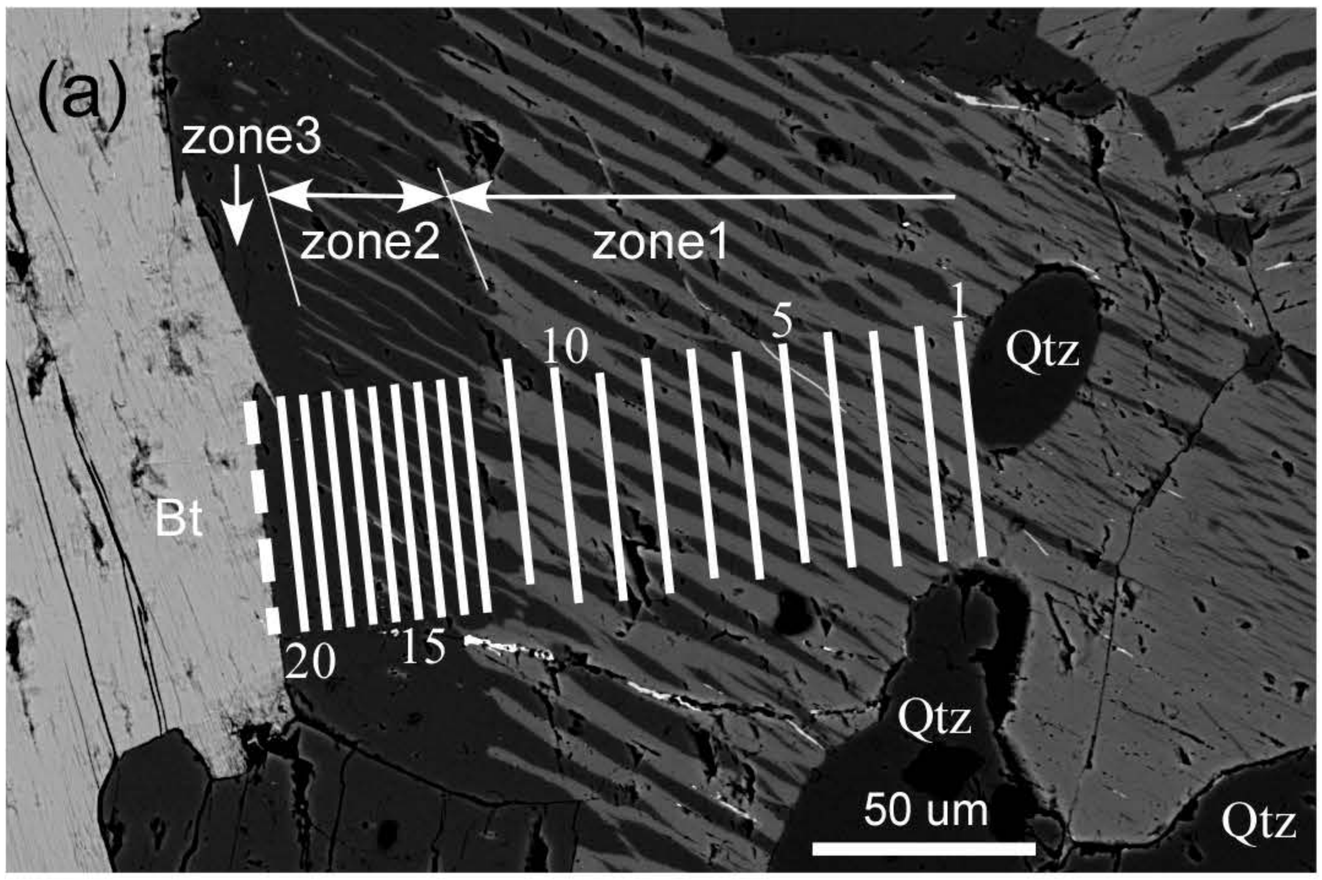

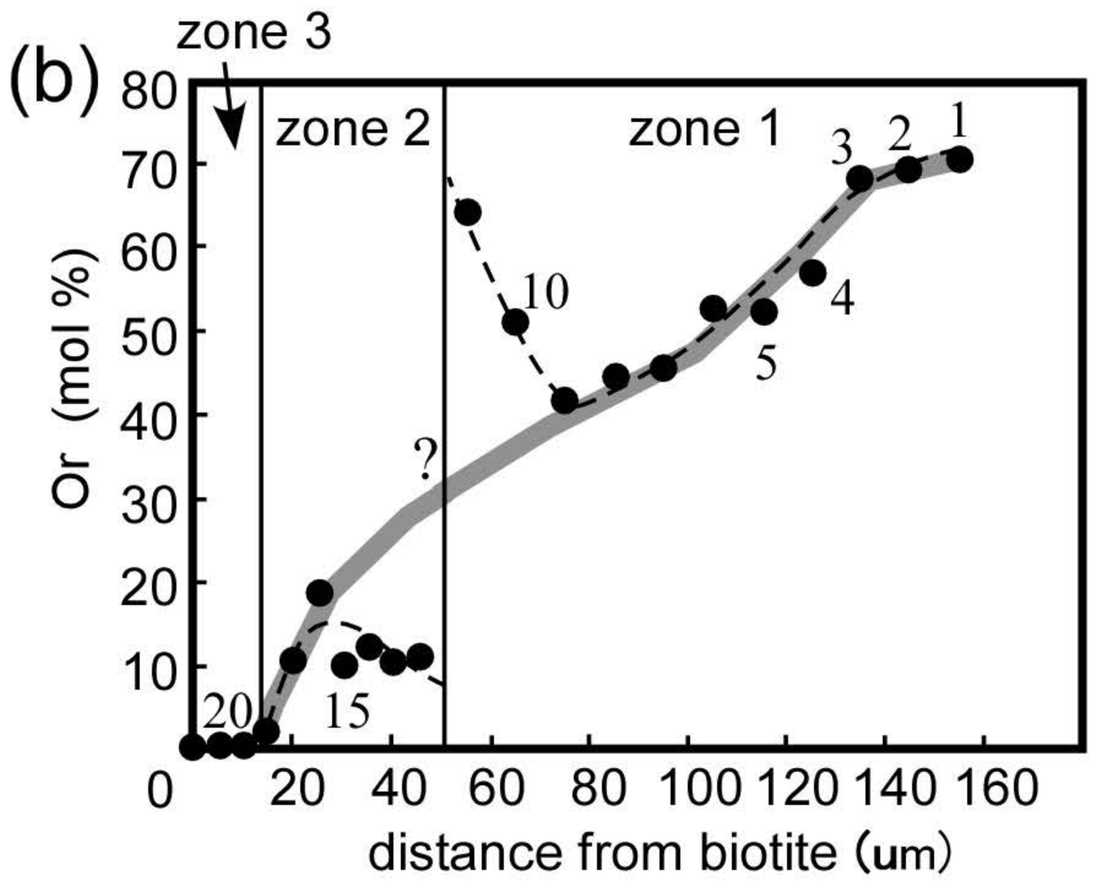

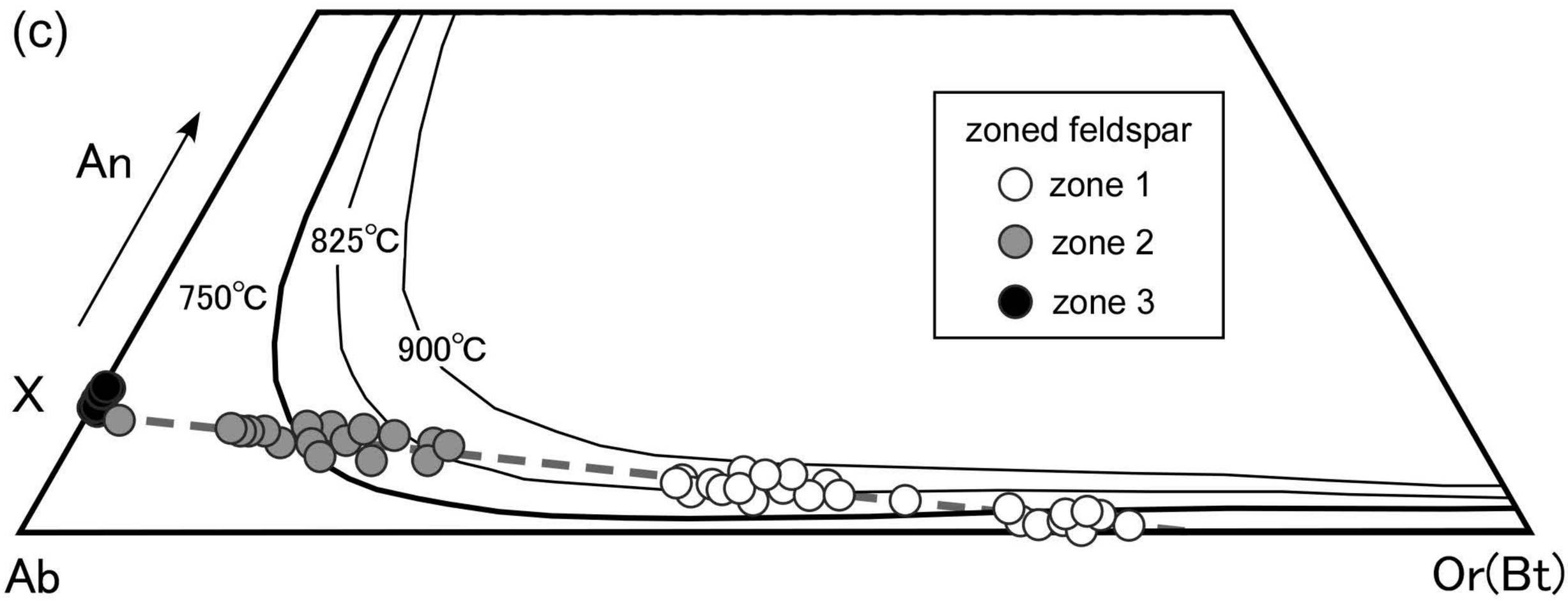

Nakamura et al. FIGURE 4

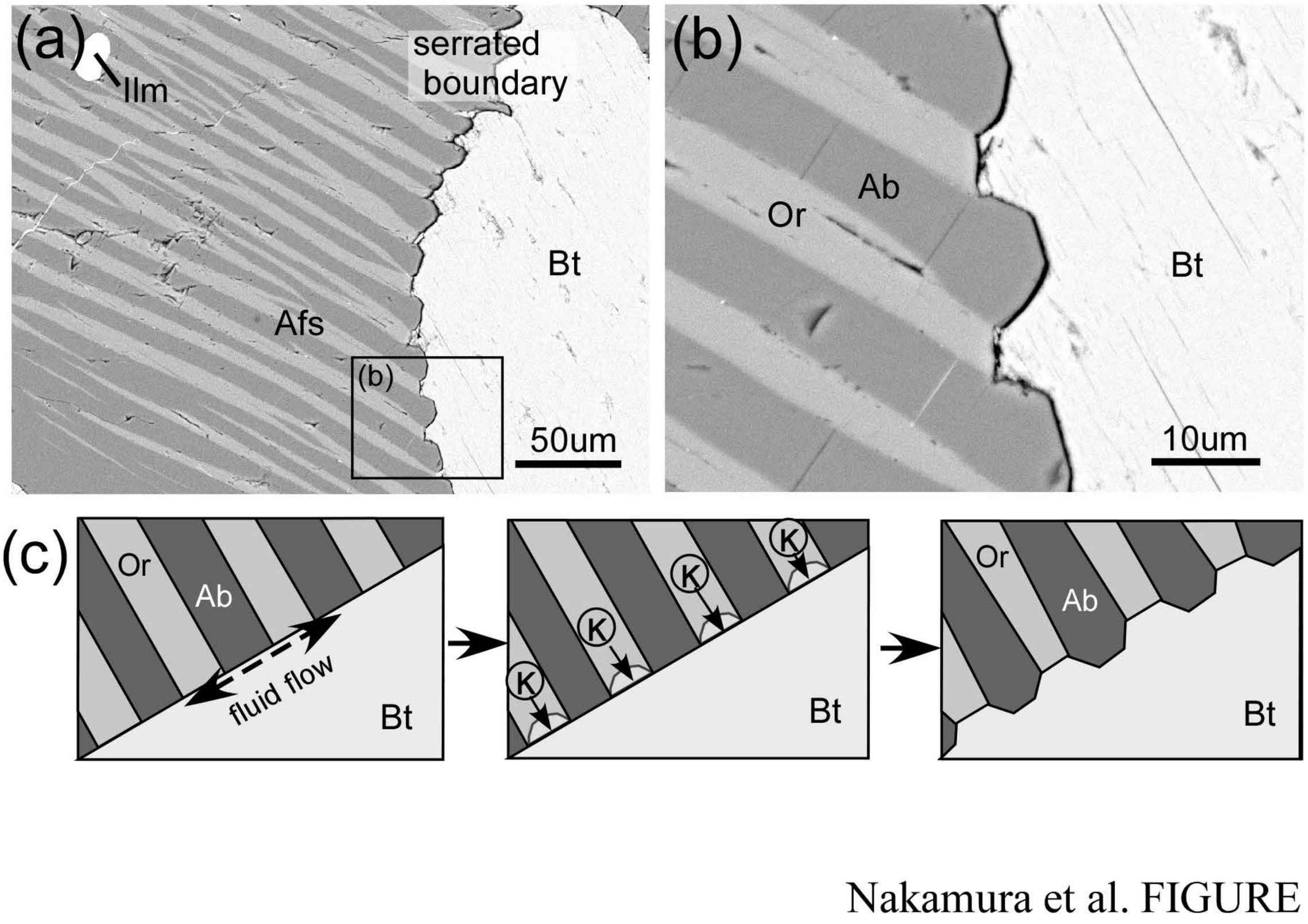

Nakamura et al. FIGURE 5

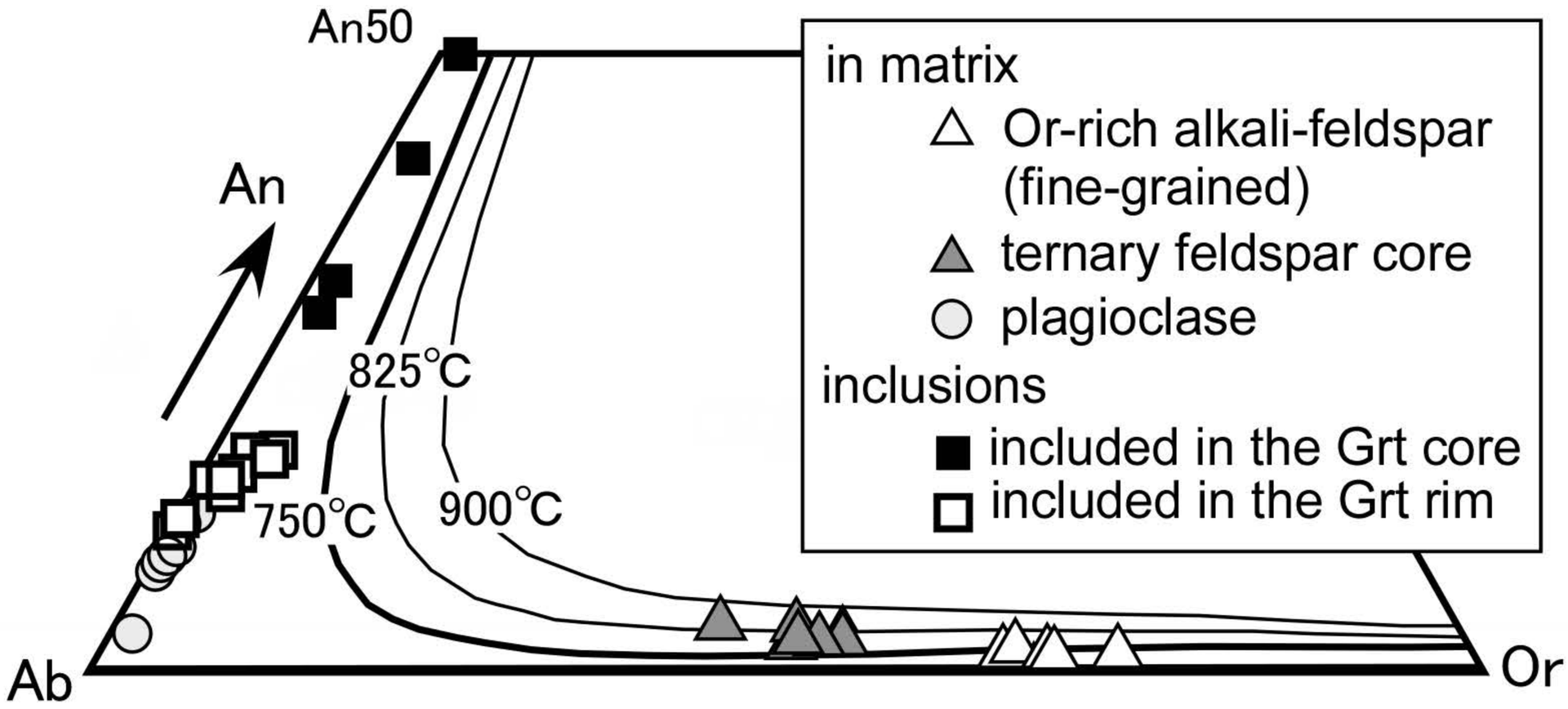

Nakamura et al. FIGURE 6

texture	ternary feldspar		Or-rich Afs rim			zoned feldspar			
zone						zone 1		zone 2	zone 3
phase	Or	Ab	Or		Ab	Or	Ab	Ab	
			average	1 S.D.					
wt%									
SiO_2	63.87	66.00	64.43	0.46	67.97	64.85	66.45	66.29	66.02
Al_2O_3	18.55	21.46	18.87	0.19	20.27	18.05	20.56	20.97	21.13
Fe_2O_3	0.00	0.00	0.02	0.02	0.05	0.02	0.07	0.04	0.00
BaO	0.61	0.09	0.32	0.08	0.00	0.56	0.00	0.08	0.00
CaO	0.01	1.61	0.16	0.04	0.40	0.01	1.90	2.06	2.20
Na_2O	1.35	10.82	3.03	0.42	11.48	0.89	10.44	10.34	10.12
K_2O	14.58	0.14	12.05	0.62	0.20	15.64	0.09	0.12	0.12
P_2O_5	0.21	0.10	0.14	0.06	0.00	0.10	0.06	0.05	0.08
Total	99.18	100.20	99.02	0.39	100.53	100.12	99.57	99.94	99.66
				formula (O = 8)					
Si	2.97	2.89	2.97		2.96	3.00	2.93	2.91	2.91
Al	1.02	1.11	1.03		1.04	0.98	1.07	1.09	1.10
Fe^{3+}	0.00	0.00	0.00		0.00	0.00	0.00	0.00	0.00
Ba	0.01	0.00	0.01		0.00	0.01	0.00	0.00	0.00
Ca	0.00	0.08	0.01		0.02	0.00	0.09	0.10	0.10
Na	0.12	0.92	0.27		0.97	0.08	0.89	0.88	0.86
K	0.87	0.01	0.71		0.01	0.92	0.01	0.01	0.01
P	0.01	0.00	0.01		0.01	0.00	0.00	0.00	0.00
Total	5.00	5.01	5.00		5.00	5.00	4.98	4.99	4.98
An	0.0	8.0	0.8		1.9	0.1	9.1	9.8	10.7
Ab	12.0	92.0	27.5		97.0	8.0	90.4	89.5	88.7
Or	88.0	1.0	71.8		1.1	92.0	0.5	0.7	0.7

Table 1 Nakamura et al.

grain name of Z.F.	zone number	Areal proportions (%)		Host and lamellae compositions						Re-integrated composition (mol%)			Equilibrium temperature (^{o}C)	
				Ab phase (mol%)			Or phase (mol%)							
		Ab phase	Or phase	An	Ab	Or	An	Ab	Or	An	Ab	Or	*T* (FL)	*T* (EG)
A	1	46.9	53.1	7.2	92.2	0.6	0.4	8.6	91.1	3.6	48.6	47.8	741	747
	2	85.1	14.9	8.2	91.1	0.7	0.4	8.6	91.1	7.0	79.2	13.8		
B	1	43.0	57.0	8.5	90.9	0.6	0.3	8.3	91.5	3.9	44.6	51.6	752	756
	2	81.2	18.8	7.4	92.4	0.2	0.3	8.3	91.5	6.1	77.1	16.8		
C	1	47.0	53.0	9.1	90.4	0.5	0.1	8.0	92.0	4.4	47.5	48.1	780	785
	2	82.1	17.9	9.8	89.5	0.7	0.1	8.0	92.0	8.1	75.4	16.5		
E	1	45.4	54.6	9.8	89.5	0.1	0.1	9.3	90.6	4.6	46.5	48.6	794	815
	2	79.1	20.9	9.8	89.6	0.7	0.1	9.3	90.6	7.8	73.3	18.9		
1	1	47.6	52.4	7.6	91.7	0.7	0.0	11.2	88.8	3.7	50.3	46.0	795	799
	2	78.9	21.1	9.1	90.6	0.3	0.0	11.2	88.8	7.2	74.3	18.4		
2	1	47.0	53.0	9.6	89.9	0.5	0.1	13.7	86.2	4.7	50.2	45.1	797	801
	2	76.9	23.1	9.6	90.1	0.4	0.1	13.7	86.2	7.4	72.9	19.6		
3	1	45.2	54.8	8.5	90.9	0.6	0.0	11.9	88.1	3.9	48.4	47.7	819	823
	2	71.3	28.7	9.3	90.2	0.5	0.0	11.9	88.1	6.7	68.3	25.0		
4	1	49.5	50.5	9.3	90.2	0.6	0.0	8.5	91.4	4.7	49.7	45.6	806	811
	2	76.7	23.3	9.6	89.9	0.5	0.0	8.5	91.4	7.5	71.5	21.0		
5	1	45.7	54.3	8.6	90.9	0.5	0.1	8.8	91.1	4.0	47.1	48.8	760	764
	2	82.4	17.6	8.4	91.1	0.4	0.1	8.8	91.1	7.0	77.1	15.9		
7	1	48.9	51.1	7.3	92.2	0.5	0.0	7.7	92.3	3.6	49.8	46.6	822	827
	2	73.6	26.4	9.0	90.7	0.4	0.0	7.7	92.3	6.7	69.4	24.0		

Table 2 Nakamura et al.